Estimation and Compensation of Doppler Effect in UAC OFDM Systems

Sadia Ahmed
Department of Electrical Engineering
University of South Florida
Email: ahmed3@mail.usf.edu

Huseyin Arslan
Department of Electrical Engineering
University of South Florida
Email: arslan@eng.usf.edu

***Abstract*—Doppler effect causes loss of orthogonality in Orthogonal Frequency Division Multiplexing (OFDM), which in turn may severely degrade receiver performance. In high data rate underwater acoustic communication (UAC), the effect of Doppler varies considerably over OFDM band. This paper will present an algorithm to avoid and/or compensate the effect of varying Doppler shift over OFDM subcarriers in order to maintain orthogonality or to compensate loss of orthogonality. To the best knowledge of the authors, the algorithm presents a novel approach to handle varying Doppler effect in UAC OFDM and thus provides valuable contribution in this domain.**

I. Introduction

In underwater acoustic communication (UAC) channel, Doppler causes significant degradation in transmission. According to literature [1], [2], the two Doppler effects, shift and spread are caused from two different sources. The *Doppler shift* is a function of the relative velocity (denoted by v_w) of the transducers/hydrophones and other objects, variable acoustic velocity (denoted by c_w), and signal frequencies. The *Doppler spread* on the other hand, is primarily caused by the wind speed on the surface waves and by the internal currents. The total Doppler effect is a combination of Doppler shift and Doppler spread, where the average Doppler shift is much larger than the overall Doppler spread [1].

In OFDM systems Doppler causes loss of orthogonality. This in turn may severely degrade receiver performance. In underwater OFDM, the bandpass frequency is comparable (for example, in Hz or kHz) to the baseband subcarrier frequencies (for example, in Hz or kHz). In such cases, the individual sub-carrier frequency variation from the bandpass frequency is significant. Therefore, the effect of Doppler shift on OFDM signal will vary over sub-carriers. The shift on the kth sub-carrier in baseband OFDM can be expressed as,

$$F_{Dkm} = \frac{v_w}{c_w} f_k cos\theta_m \ , \tag{1}$$

where f_k is the kth sub-carrier frequency, θ_m is the scattering angle of the mth scatterer, c_w is the sound speed in water, and v_w is the mobile velocity in water. Compared to the narrowband terrestrial, Doppler in UAC is more severe. This is primarily due to, A) Very low acoustic velocity compared to RF velocity, c_a i.e. $c_w << c_a$) giving rise to high Doppler effect, B) The comparable Doppler amount to the low values of sub-carrier frequencies, and C) The variable Doppler effect over subcarriers due to low bandpass frequencies. Fig. 1 illustrates the varying effect of Doppler shift over OFDM

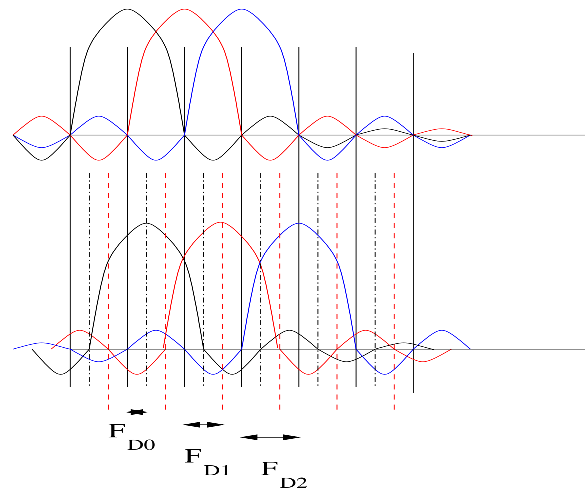

Fig. 1. Varying Effect of Doppler Shift over OFDM Sub-carriers

sub-carriers. A detailed evaluation results of varying Doppler effect in frequency domain for UAC OFDM systems has been presented in [3].

This paper will propose an algorithm to estimate the varying effects of Doppler shift over subcarriers and to mitigate the ICI produced by such effects in the frequency domain. The proposed algorithm will utilize the variable sub-carrier spacing and signal to interference ratio (SIR) over sub-carriers to maintain orthogonality by avoiding ICI or compensate loss of orthogonality by compensating ICI. Simulation will be carried out using simulated Rayleigh channel and realistic channel responses. Although, due to lack of standard channel models, the number of realizations in actual UAC channels is limited. Acoustic velocity variation is also considered in the UAC simulation.

The proposed algorithm improves receiver performance when compared to the performance in the absence of avoidance and/or compensation technique. To the best knowledge of the authors, this type of compensation algorithm has not been presented in UAC OFDM and thus provides a valuable contribution.

The rest of the paper is organized as follows. In Section II, the analysis of Doppler effect is presented. In Section III, the algorithm to avoid and/or to compensate Doppler effect is presented. In Section IV, the simulation result is provided

978-1-4244-5222-4/10/$26.00 ©2010 IEEE

and in Section V, the concluding remarks are presented.

II. Analysis

The evaluation of Doppler effect and frequency offset in UAC OFDM systems is covered in [3]. For the convenience of the reader a part of that analysis corresponding to Doppler effect is presented here without going into detail.

Channel Model: A frequency selective and time varying channel can be expressed as (according to [4]),

$$h(t,\tau) = \sum_{l=0}^{L-1} \alpha_l(t,\tau)\delta(\tau - \tau_l(t)), \tag{2}$$

where $\alpha_l(t,\tau)$ and $\tau_l(t)$ represent the attenuation coefficient and the path delay of the lth delay bin respectively. Both parameters are function of time and depend on the scatterers arriving within the lth bin. The variable L represents the total number of multipaths or delay bins and δ represents the Dirac Delta function. In a flat and fast fading channel, the time varying channel impulse corresponding to one delay bin can be expressed as,

$$\begin{aligned} h(nT_s) &= \sum_{m=0}^{M-1} a_m(nT_s)\delta(nT_s - \tau_m(nT_s)) \\ &= \sum_{m=0}^{M-1} h_m(nT_s), \end{aligned} \tag{3}$$

where $a_m(nT_s)$ and $\tau_m(nT_s)$ are the time varying complex gain and the delay of the mth scatterer within the bin. The variable T_s denotes the sampling period, nT_s represents the time corresponding to the nth sample, $h_m(nT_s)$ represents the discrete time based channel impulse of the mth scatterer, and M denotes the total number of scatterers within the bin. Throughout the rest of the analysis, n will be used in place of nT_s.

The channel impulse $h(n)$ is a complex quantity. It can be assumed that the real and imaginary components of $h(n)$ are independent and identically distributed (i.i.d.) with Gaussian distribution. Under such condition, the modulus of $h(n)$ or $|h(n)|$ will follow Rayleigh distribution [4]. Each scatterer causes a Doppler shift while M scatterers arriving at the same instance within the delay bin will cause Doppler spread. Considering M number of time samples corresponding to M scatterers and using (3), the kth channel frequency sample can be expressed as (similar to [5]),

$$\begin{aligned} H_k(n) &= \sum_{m=0}^{M-1} h_m(n) e^{-j2\pi\frac{mk}{N}} \\ &= \sum_{m=0}^{M-1} h_m(n) e^{-j2\pi f_k(mT_s)}, k = 0,1,...,M-1. \end{aligned} \tag{4}$$

Although flat fading channel is considered in the above analysis, the same can be extended to frequency selective channels.

OFDM Signal Structure: After performing inverse fast Fourier transform (IFFT) on the frequency domain OFDM signal, the nth discrete time sample of the transmitted signal can be expressed as,

$$X_n = \sum_{k=0}^{N-1} X_k e^{j2\pi\frac{nk}{N}} \quad 0 <= n <= N-1. \tag{5}$$

Replacing nk/N in (5),

$$X_n = \sum_{k=0}^{N-1} X_k e^{j2\pi f_k(nT_s)} \quad 0 <= n <= N-1, \tag{6}$$

where the real and imaginary components of the complex signal X_n are assumed to be i.i.d. Gaussian distributed [6]. If the channel is frequency selective, an additional cyclic prefix (CP) of length G will be added to each OFDM symbol such that, $G >= M$. The transmitted signal with CP can be expressed as (similar to [5]),

$$X_n = \sum_{k=0}^{N-1} X_k e^{j2\pi f_k(nT_s)} \quad -G <= n <= N-1,$$

where the extra prefix symbols are denoted as $X_n = X_{N+n}, n = -G, ..., -1$. After the removal of the cyclic prefix, the signal will deduce to (6).

Received OFDM Signal: The received OFDM signal Y_n can be expressed as a discrete convolution between the transmitted signal and the channel (similar to [5],[7]),

$$Y_n = \sum_{m=0}^{M-1} h_m(n) X_{n-m} \quad 0 <= n <= N-1, \tag{7}$$

where the n in $h_m(n)$ denotes the time variation of the mth scatterer. After performing fast Fourier transform (FFT) on the time domain received signal, the frequency domain signal can be expressed as, $Y_k = \sum_{n=0}^{N-1} Y_n e^{-j2\pi\frac{nk}{N}}$. Using (7) in Y_k,

$$Y_k = \sum_{n=0}^{N-1} \Big[\sum_{m=0}^{M-1} h_m(n) X_{n-m}\Big] e^{-j2\pi\frac{nk}{N}}. \tag{8}$$

Using (6) in (8),

$$Y_k = \sum_{n=0}^{N-1} \underbrace{\Big[\sum_{m=0}^{M-1} h_m(n)\Big(\sum_{k=0}^{N-1} X_k e^{j2\pi(f_k)(n-m)T_s}\Big)\Big]}_{A} \cdot e^{-j2\pi f_k(nT_s)}. \tag{9}$$

The time variation of the mth scatterer will cause phase variation of the received OFDM signal and in turn will result in a frequency shift. Incorporating this frequency shift into the channel impulse, (3) can be expressed as linear time-variant filter with complex response of,

$$\begin{aligned} h(n) &= \sum_{m=0}^{M-1} a_m e^{-j\phi_m(nT_s)}\delta(nT_s - \tau_m) \\ &= \sum_{m=0}^{M-1} a_m e^{-j\phi_m(nT_s)}\delta(nT_s - mT_s), \\ &= \sum_{m=0}^{M-1} h_m e^{-j\phi_m(nT_s)}, \end{aligned} \tag{10}$$

where $\phi_m(nT_s) = 2\pi[(f_k + f_{km})(nT_s - \tau_m)]$ [6] [8]. The variable f_{km} is the Doppler shift on the kth subcarrier due to the mth scatterer and is represented as,

$$f_{km} = (f_0 + k\Delta f)\frac{v_w}{c_w}cos\theta_m, \tag{11}$$

where f_0 is the lowest subcarrier frequency and Δf is the subcarrier spacing. Using (10) in (4) and after some simple computation,

$$H_k(n) = \sum_{m=0}^{M-1} h_m e^{-j2\pi(f_k(nT_s)+f_{km}(n-m)T_s)}. \tag{12}$$

The A of (9) can be expanded using (10) and is presented in the appendix of [3]. After some simple computation, the received signal can be expressed as,

$$Y_k = \underbrace{\sum_{n=0}^{N-1} X_k H_k(n)}_{Desired} + \underbrace{\sum_{n=0}^{N-1}\sum_{p=0,p\neq k}^{N-1} X_p H_p(n)\cdot e^{j2\pi(f_p-f_k)(nT_s)}}_{ICI}, \tag{13}$$

where both the desired and the ICI are complex values incorporating time varying channel.

ICI and SIR: Taking into account an additive white Gaussian noise (AWGN) term with zero mean and variance of σ_{noise}, the signal to interference plus noise ratio (SINR) can be expressed as,

$$\begin{aligned} SINR_{ICIDoppler} &= \frac{Signalpower}{ICIpower + noisepower} \\ &= \frac{E|Desired|^2}{E|ICI|^2 + \sigma_{noise}}, \end{aligned} \tag{14}$$

where after some computation [3], the $|ICI|^2$ can be expressed as,

$$\begin{aligned} |ICI|^2 &= \Big| \sum_{n=0}^{N-1} X_0 H_0 . e^{-j2\pi(k\Delta f)(nT_s)} \dots \\ &+ \sum_{n=0}^{N-1} X_p H_p . e^{-j2\pi((k-p)\Delta f)(nT_s)} \dots \\ &+ \sum_{n=0}^{N-1} X_{N-1} H_{N-1} . e^{-j2\pi((k-N+1)\Delta f)(nT_s)} \Big|^2 \end{aligned} \tag{15}$$

When only signal to interference ratio (SIR) is considered (14) becomes,

$$\begin{aligned} SIR_{ICIDoppler} &= \frac{Signalpower}{ICIpower} \\ &= \frac{E|Desired|^2}{E|ICI|^2}. \end{aligned} \tag{16}$$

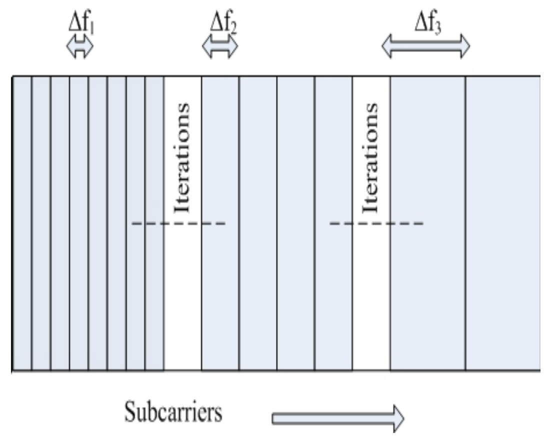

Fig. 2. Signal Structure: ICI Avoid: Sub-carrier Spacing Adjustment

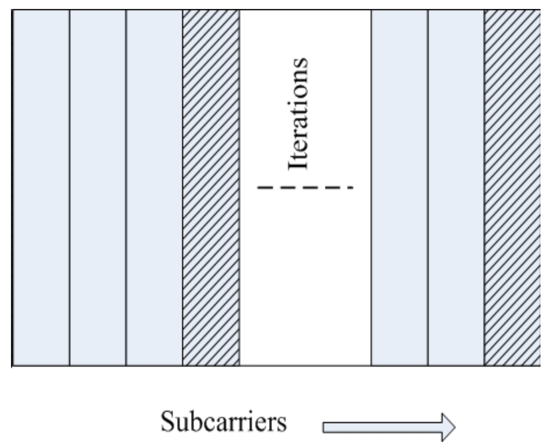

Fig. 3. Signal Structure: ICI Compensate: Omit Sub-carriers

III. Proposed Algorithm

A. Proposed Signal Architecture

The proposed algorithm applies the avoidance and compensation mechanism in the frequency domain. Therefore, determining Doppler scale factor and re-sampling in the time domain as in [9]-[11] does not apply. When Δf is adjusted, the signal structure may be represented as Fig. 2 similar to [12]. In each iteration, the subcarrier spacing may be increased or decreased depending on the data rate threshold. When any sub-carrier with the lowest SIR is dropped, the structure can be illustrated in Fig. 3. After comparing the lowest SIR to the SIR threshold, the lowest SIR may be dropped in each iteration.

B. Algorithm

The proposed algorithm compensate ICI induced by Doppler shift in the frequency domain. The Doppler shift is assumed non-varying over each OFDM block but its effect varies over the OFDM sub-carriers.

In the initialization phase,

- Determine carrier spacing, $\Delta f = \frac{1}{T_{OFDM}}$ (with no ICI), where T_{OFDM} represents the OFDM symbol duration.
- Determine minimum allowable sub-carrier spacing, Δf_{MIN}, which will produce ICI and in turn, is a function of tolerable SIR threshold, SIR_{TH} at the receiver.
- Determine minimum allowable data rate threshold, $RATE_{TH}$.

From the received signal,

1) Calculate overall data rate, $RATE_{All}$.
2) Calculate SIR per sub-carrier
   Loop ii=1:N
      Calculate SIR_{ii} for each sub-carrier
      Sort and Store all SIR per sub-carrier.
      Determine minimum $SIR_{ii_{MIN}}$
   End loop
3) **If** $SIR_{ii_{MIN}} >= SIR_{TH}$ and $RATE_{All} >= RATE_{TH}$
   No further avoidance or compensation needed.
   Move to step 5
   end if
4) **If** $SIR_{ii_{MIN}} < SIR_{TH}$
   First method adjust carrier spacing...
      Increase Δf to $\Delta f'$.
      Calculate data rate, $RATE_{All}$.
      If $RATE_{All} >= RATE_{TH}$
         Repeat steps from 2 with $\Delta f'$.
      else
   Second method drop sub-carrier...
         Drop Mth sub-carrier corresponding to SIR_{MIN}
         $N = N - 1$
         Repeat steps from 2 with Δf
      end if.
   else
   Carrier spacing needs to be adjusted...
      Decrease Δf to $\Delta f''$ such that $\Delta f'' >= \Delta f_{MIN}$
      Calculate data rate, $RATE_{All}$.
      Repeat steps from 2 with $\Delta f''$
   end if
5) **EXIT**

C. Discussion

The algorithm adaptively adjusts subcarrier spacing and subcarriers to accommodate change in ICI due to change in Doppler shift for specific OFDM bandwidths (BW). If the FFT points are increased in order to increase data rate, the ICI may increase and hence the SIR may decrease. If the subcarrier spacing is increased, the ICI may reduce and that may increase SIR, but the data rate may decrease. From the equations in section II, it can be seen that the SIR and hence the SIR_{TH} is primarily a function of subcarrier spacing, OFDM BW, FFT points, sound speed, mobile velocity, and subcarrier frequency.

The desired signal power may also be affected by frequency distortion due to Doppler shift and may be observed in equations (12) and (13). The frequency distortion may cause the desired signal not to be sampled at the signal peak for each subcarrier.

The more the variation and availability of possible choices of FFT points, the more flexible will be the choice of data rate, and the more adaptive will the algorithm will be. When one or more subcarriers are dropped, the overall data rate may be affected as well. For the simplicity of analysis and comparison, absence of pilot and guard carriers is assumed.

IV. Simulation Results

The simulation is carried out using the parameters in Table I. The results are provided for simulated Rayleigh channel and for realistic underwater acoustic channel responses. In UAC, standard channel models are not available for various ocean locations and channel conditions. Therefore, a generic simulated Rayleigh channel is necessary.

A. *Simulated Channel:*

Each individual scatterer is a complex quantity with the real and imaginary components being i.i.d. Gaussian. With that in mind, the real and imaginary components of each scatterer are generated using normally distributed random numbers. The delays are also generated as normally distributed random numbers. The incident angle θ_m is represented by uniform distribution according to modified Jake's model. Since the simulation is carried out for flat fading, 2-Ray Rayleigh model does not apply here. The equations (13), (15), and (16) are used in the simulation.

In UAC, the values of $\alpha_l(t, \tau)$ and $\tau_l(t)$ of (2) can be considered as random, since the geometry of the ocean floor, surface waves, internal current, and the movement of the transducers, that cause time varying multipaths are all random [1].

Fig. 4 represents the average ICI power for each subcarrier owing to Doppler shift in a simulated UAC channel for 128 FFT points, for a bandwidth of 10 kHz, and for two different acoustic velocities. For BPSK modulation scheme, the FFT point represents the total number of samples and the overall data rate becomes 128. Let the $RATE_{TH}$ be equal to 64 in this case. The Doppler shift and hence the ICI for sound speed of 1550 m/sec is less than the shift and ICI for speed of 1450 m/sec. This can be observed in the figure where the ICI in the latter case is more than the ICI in the former. Consequently, the SIR_{MIN} will be less for speed of 1450 m/sec. In the case of 1550 m/sec, if it is assumed that the SIR_{TH} is satisfied and since the data rate of $128 > RATE_{TH}$ is also satisfied, at step (3), the algorithm will exit and will not need to continue. In the case of 1450 m/sec, even though the SIR_{MIN} may decrease, if it is assumed that it is still greater or equal to SIR_{TH}, then step (3) will still satisfy and the algorithm will exit.

Fig. 5 represents the average ICI power for each subcarrier for 128 FFT points, for a bandwidth of 100 kHz, and for two different acoustic velocities. The FFT point represents the total number of samples and the overall data rate is 128. Let the $RATE_{TH}$ be equal to 128 in this case. The ICI for sound speed of 1550 m/sec is slightly less than the ICI for speed of 1450 m/sec. Consequently, the SIR_{MIN} will be slightly less for speed of 1450 m/sec. In the 1550 m/sec case, if it is assumed that the SIR_{TH} is satisfied and since the data rate of $128 = RATE_{TH}$ is also satisfied, at step (3), the algorithm will exit and will not need to continue. In the case of 1450 m/sec, even though the SIR_{MIN} may decrease slightly, both conditions of step (3) may still satisfy and the algorithm will exit.

The 100 kHz BW is larger than 10 kHz and hence ICI in general for 100 kHz is slightly less than that for 10 kHz for the same data rate of 128. This is due to the increase in Δf for 100 kHz band compared to 10 kHz band for the same FFT points.

In each case of the above two BW, the algorithm adapts to the Doppler shift change, which in this example is caused by the change in sound velocity. The change in SIR (due to change in ICI), which is due to change in Doppler shift, causes the algorithm to re-evaluate the SIR and data rate. In the above scenarios, changing Δf or dropping of subcarrier was not required.

Fig. 6 represents the average ICI power for 128 FFT points, for a bandwidth of 100 Hz, and for two different acoustic velocities. Let the $RATE_{TH} = 64$. Since the frequencies are lower for 100 Hz BW, a reduction in sound speed to 1450 m/sec from 1550 m/sec may not make much change in Doppler shift and ICI for both sound velocities almost overlap each other.

For both sound speeds the ICI is high and consequently, SIR_{MIN} will be low. The $128 > RATE_{TH}$, but if $SIR_{MIN} < SIR_{TH}$, at step (3) of the algorithm, both conditions will not satisfy and step (4) of the algorithm will be accessed. In this step, Δf will need to increase. Let the new data rate or $RATE_{All} = 64$. The new $RATE_{All} = RATE_{TH}$ and therefore, this new Δf is used in recalculating the ICI (and in turn, the SIR) as seen in Fig. 7. The ICI is reduced in Fig. 7 in comparison to Fig. 6 for both sound speeds. In step (3) both conditions, $SIR_{MIN} >= SIR_{TH}$ and $RATE_{All} = RATE_{TH}$ will satisfy and the algorithm will exit.

Compared to 10 kHz and 100 kHz bandwidths, ICI is relatively higher in 100 Hz BW for the same data rate of 128. It is expected because the same FFT points in a smaller BW may produce greater Doppler shift effect and hence more ICI.

Fig. 8 represents the average ICI power for 128 and 64 FFT points, for a bandwidth of 1000 kHz and for sound speed of 1550 m/sec. Let the $RATE_{TH} = 128$. Let the $RATE_{All}$ be 64. In step (3), $RATE_{All} < RATE_{TH}$ and $SIR_{MIN} >= SIR_{TH}$ and therefore, step (4) will be accessed. In step 4, the algorithm will decrease Δf and re-calculate $RATE_{All} = 128$. After calculating the new SIR_{ii} in step (2), the ICI power plot is presented for 128

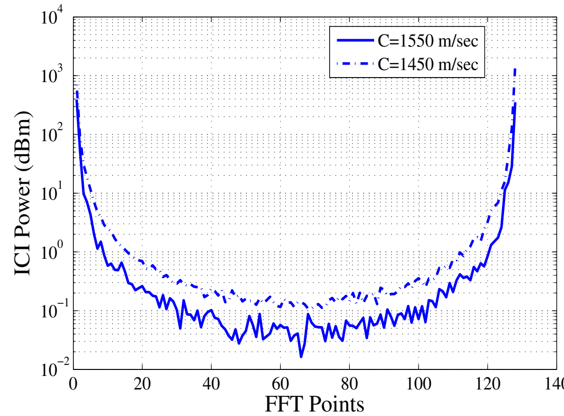

Fig. 4. ICI Power in Simulated UAC Channel for FFT=128, Bandwidth=10kHz, Minimum Frequency=10kHz, Maximum Frequency=20kHz, and Mobile Velocity=5 m/sec

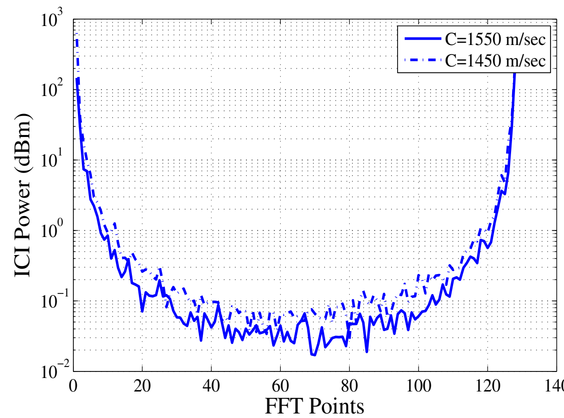

Fig. 5. ICI Power in Simulated UAC Channel for FFT=128, Bandwidth=100kHz, Minimum Frequency=100kHz, Maximum Frequency=200kHz, and Mobile Velocity=5 m/sec

FFT points in Fig. 8. In step (3), $RATE_{All} = RATE_{TH}$, and if $SIR_{MIN} >= SIR_{TH}$ satisfies, then the algorithm will exit. However, if $SIR_{MIN} >= SIR_{TH}$ does not satisfy, then the subcarrier with SIR_{MIN} can be dropped in step (4).

B. *Actual Channel:*

The channel impulse response from [13] is used for the UAC systems. Fig. 9 represents the average ICI power for each subcarrier owing to Doppler shift in an actual UAC channel for 64 FFT points, for a bandwidth of 100 Hz, and for two different acoustic velocities. The SIR resulting from ICI is within threshold for both sound speeds similar to the simulated channel in Fig. 7. If $RATE_{TH} = 64$ then in step (3) both conditions, $SIR_{MIN} >= SIR_{TH}$ and $RATE_{All} = RATE_{TH}$ will satisfy and the algorithm will exit.

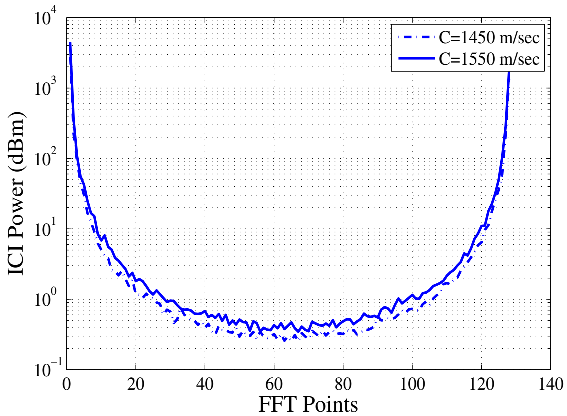

Fig. 6. ICI Power in Simulated UAC Channel for FFT=128, Bandwidth=100Hz, Minimum Frequency=100Hz, Maximum Frequency=200Hz, and Mobile Velocity=5 m/sec

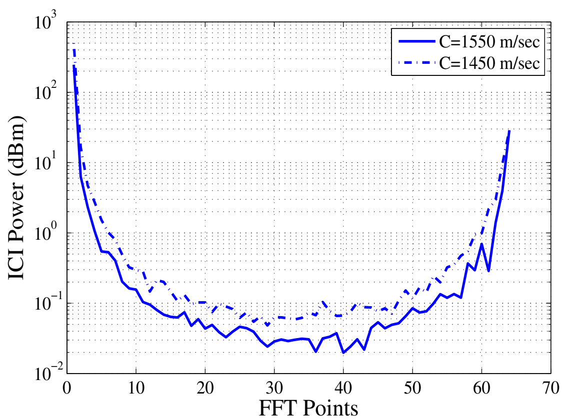

Fig. 7. ICI Power in Simulated UAC Channel for FFT=64, Bandwidth=100Hz, Minimum Frequency=100Hz, Maximum Frequency=200Hz, and Mobile Velocity=5 m/sec

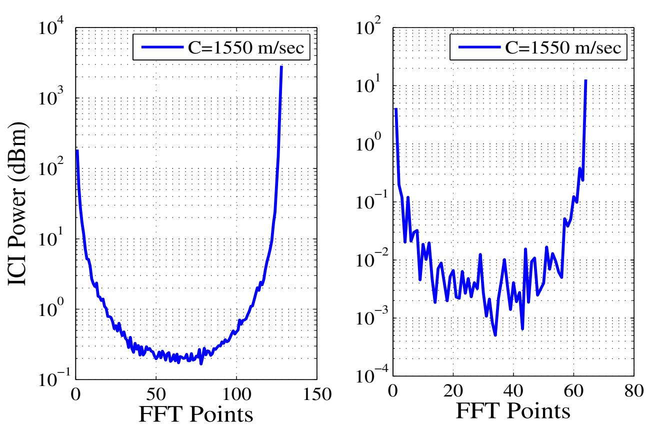

Fig. 8. ICI Power in Simulated UAC Channel for FFT=128 (left),FFT=64 (right), Bandwidth=1000kHz, Minimum Frequency=10kHz, Maximum Frequency=1010kHz, and Mobile Velocity=5 m/sec

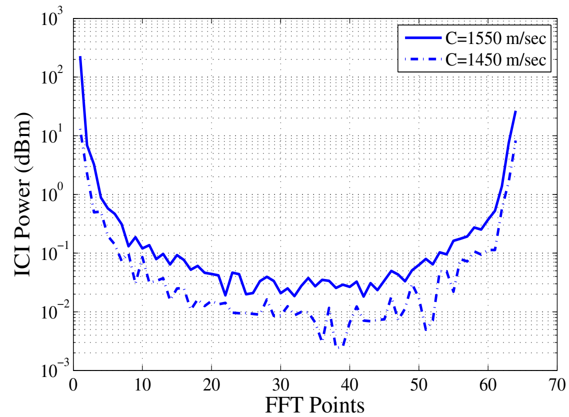

Fig. 9. ICI Power in Actual UAC Channel for FFT=64, Bandwidth=100Hz, Minimum Frequency=100Hz, Maximum Frequency =20Hz, and Mobile Velocity=5 m/sec

TABLE I
SIMULATION PARAMETERS

Parameters	Values
Frequency(min)(kHz)	100Hz,10,100,10
Frequency(max)(kHz)	200Hz,20,200,1010
Bandwidth(kHz)	100Hz,10,100,1000
FFT Size	64,128
TxRx Speed(m/sec)	5
Signal Velocity(m/sec)	1450,1550
Realizations	1000
Channel	Rayleigh,Actual

V. CONCLUSION

Doppler effect varies considerably over OFDM sub-carriers in UAC OFDM. This produces varying ICI over OFDM sub-carriers. In this paper, an algorithm is presented to tackle such varying Doppler effect in frequency domain. The ICI is handled by changing sub-carrier spacing, and in turn changing FFT points and/or by removing sub-carriers that have lower than threshold signal to interference ratio. This way the receiver is able to adapt to Doppler shift and hence to the ICI changes.

REFERENCES

[1] B. Kim and I. Lu, "Parameter study of OFDM underwater communications system," in *Proc. IEEE OCEANS*, vol. 2, 2000.

[2] M. Stojanovic, "Recent advances in high-speed underwater acoustic communications," *IEEE J. of Oceanic Engineering*, vol. 21, no. 2, pp. 125–136, 1996.

[3] S. Ahmed and H. Arslan, "Evaluation of Frequency Offset and Doppler Effect in Terrestrial RF and Underwater Acoustic OFDM Systems," in *Proc. IEEE The Military Communicatins Conference, MILCOM*, 2008.

[4] T. S. Rappaport, *Wireless Communications: principles and practice, Pearson Education, Ed. Delhi, India: Pearson*. Pearson, 2002, ch. 5, Mobile Radio Propagation: Small-Scale Fading and Multipath, pp. **5**–182 – **5**–212.

[5] R. Y. Yen, H. Y. Liu, and W. Tsai, "QAM Symbol Error Rate in OFDM Systems Over Frequency-Selective Fast Ricean Fading Channels," *IEEE Tran. Vehicular Technology*, 2003.

[6] I. Capoqlu, Y. Li, and A. Swami, "Effect of Doppler spread in OFDM-based UWB systems," *IEEE Tran. Wireless Communications*, pp. 2559–2567, Sept. 2005.

[7] Y. Mostofi and D. Cox, “ICI Mitigation for Pilot-Aided OFDM Mobile Systems,” *IEEE Tran. Wireless Communications*, vol. 4, no. 2, pp. 765–774, 2005.

[8] G. L. Stuber, *Mobile Communication: Principles of*, ch. 2, Propagation Modeling, pp. **2**–39 – **2**–43.

[9] A. Salberg and A. Swami, “Doppler and frequency-offset synchronization in wideband OFDM: Estimators and performance analysis,” *IEEE Tran. Wireless Communications*, Nov. 2005.

[10] B. Li, S. Stojanovic, M. Freitag, and P. Willett, “Non-Uniform Doppler Compensation for Zero-Padded OFDM over Fast-Varying Underwater Acoustic Channels,” in *Proc. IEEE OCEANS*, 2007, pp. 1–6.

[11] Stojanovic, “Low Complexity OFDM Detector for Underwater Acoustic Channels,” in *Proc. IEEE OCEANS*, Boston, MA, Sept. 2006, pp. 1–6.

[12] S. Das, E. De Carvalho, and R. Prasad, “Dynamically Adaptive Bandwidth for Sub Carriers in OFDM Based Wireless Systems,” in *Proc. IEEE Wireless Communications and Networking Conference, WCNC*, 2007, pp. 1378–1383.

[13] M. Chitre, J. Potter, and O. Heng, “Underwater acoustic channel characterisation for medium-range shallow water communications,” in *Proc. IEEE OCEANS*, Nov 2004, pp. 9–12.